Current-Excitation Based ΔR-to-Frequency Converter for Resistive Sensors

Ekta Sharma, Meraj Ahmad, Anwar Ulla Khan, Laxmeesha Somappa, Maryam Shojaei Baghini, Hadi Heidari, and Shahid Malik.

***Abstract*— This paper presents a relaxation oscillator-based high-resolution resistance measurement system. The proposed signal conditioning circuit utilizes a half-bridge topology with a bi-directional current excitation. The circuit modulates the incremental change in the sensor resistance in the form of a change in the frequency of the relaxation oscillator. The baseline resistance of the sensor is automatically compensated using a digital potentiometer at the beginning of the measurement cycle. The proposed circuit is analyzed in detail by considering the non-idealities of the circuit components. The design consideration is provided for different components. A prototype PCB of the proposed circuit is developed. The results show that the proposed circuit can provide a signal-to-noise ratio of 80 dB for a wide-range incremental change in the sensor resistance up to 500 kΩ with an error of less than ± 1%. The developed board is tested with humidity sensors. The result confirms the efficacy of the proposed circuit for a wide measurement range.**

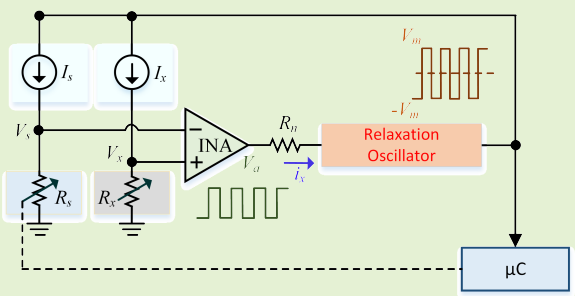

***Index Terms*— Resistive sensors, resistance-to-frequency converter, temperature sensor, humidity sensor, interface electronic circuits, half-bridge, high resolution, high accuracy.**

I. Introduction

RESISTIVE sensors are widely used in industrial, automation, scientific, health-care, environmental, and agriculture applications for sensing various chemical, physical, and biological parameters such as displacement, pressure, force, temperature, gas concentration, body temperature, respiration rate, micro-droplet, and soil moisture content [1]–[4].

The resistive sensor systems consist of mainly three blocks: (i) the resistive sensor, (ii) the signal conditioning circuit, and (iii) the data acquisition unit [5]. The resistive sensors have a fixed baseline resistance (R_s) and an incremental change in the resistance (ΔR) due to measurand. The value of ΔR is small compared to R_s, affecting the measurement system's resolution and dynamic range [2], [6]. The signal conditioning circuits convert the sensor's resistance into a form suitable for the data acquisition unit. This signal conditioning circuit may involve amplification, filtering, linearization, and baseline cancellation. The data acquisition unit is another crucial aspect of the sensor system since it can be seen as the stage where the measurement is actually performed [7].

The Wheatstone bridge-based signal conditioning circuits are widely used for resistive sensors. The full and half Wheatstone bridge configuration, followed by an instrumentation amplifier, provides linear output voltage with high sensitivity for resistive sensors. However, the Wheatstone bridge-based circuits are not suitable for the single-element resistive sensors due to the non-linear output voltage with respect to the measurand. Auto-nulling loop-based signal conditioning circuits are designed for linearizing the output voltage of the single-element Wheatstone bridge [8], [9]. However, the auto-nulling loop requires additional components, such as an integrator and analog multiplier, which increases the complexity and power consumption of the signal conditioning circuits [10], [11]. The output of the Wheatstone bridge-based circuits is mostly analog voltage signals. An analog-to-digital converter (ADC) is needed as the data acquisition unit for such circuits.

In addition to the non-linearity issue, the accuracy of the analog output of the Wheatstone bridge-based circuits for single-element resistive sensors degrades significantly in the case of distant transmission. Therefore, the physical location of the data acquisition unit becomes very important, particularly in distributed sensing systems. Presently, smart sensor systems with onboard ADC are available in the market. However, there are still cases where technical and economic constraints make performing the conversion remotely from sensors desirable, and analog signal transmission is preferred in such cases. On the other hand, if such requirements are not critical, the digital data is transmitted as it is easy to maintain signal integrity in digital data [12].

In such cases, the oscillator-based circuits with square-wave output are preferred where the sensor information is

Ekta Sharma and Shahid Malik are with the Centre for Sensors, Instrumentation, and Cyber-Physical System Engineering, Indian Institute of Technology Delhi - New Delhi, 110016, India.
Laxmeesha Somappa and Maryam Shojaei Baghini are with the Department of Electrical Engineering, Indian Institute of Technology Bombay, Mumbai- 400076, India.
Meraj Ahmad and Hadi Heidari are with the James Watt School of Engineering, University of Glasgow, United Kingdom.

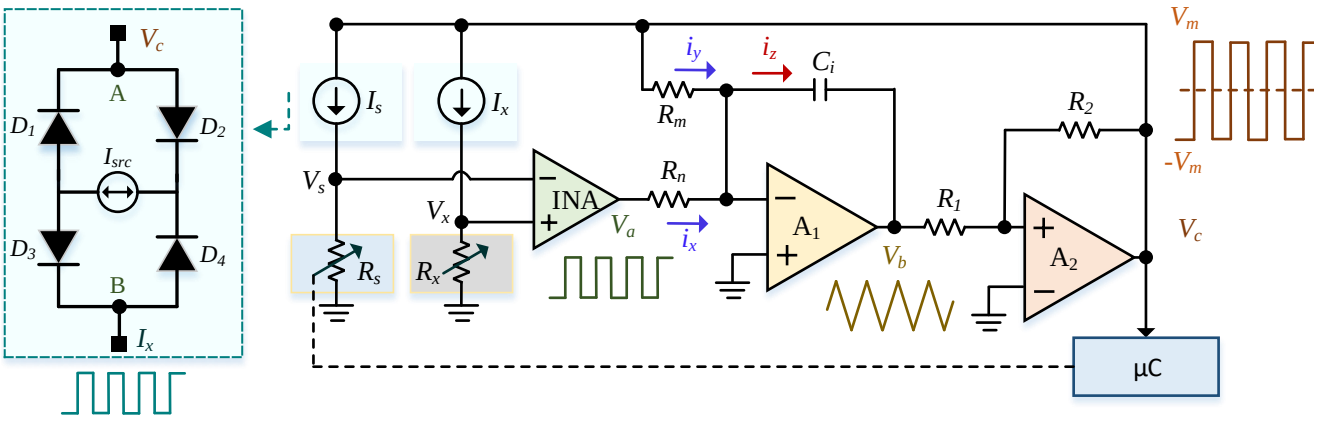

Fig. 1. The schematic diagram of the proposed signal conditioning circuit- the first proposed interface. The schematic in the dotted box shows the diode-based bidirectional current generator.

modulated on the time scale, such as frequency, time period, and duty cycle. The quasi-digital nature of the square-wave output of the oscillator avoids the need for an ADC and provides excellent noise-immunity and high resolution for the slow varying measurands [13]–[18].

This paper presents a relaxation oscillator-based ΔR-to-frequency converter for resistive sensors. The proposed circuit utilizes a half-bridge-based topology, which provides linear output voltage with respect to the measurand for single-element resistive sensors. Compared with the previously reported resistance-to-frequency converter, the main contributions of the proposed circuit are as follows:

1) Half-Bridge Topology: The Wheatstone-bridge-based resistance-to-frequency converters reported in [19]–[21] needs the manual calibration of three resistors of the bridge for baseline resistance cancellation. In comparison, the proposed circuit utilizes a half-bridge topology which allows the compensation of the effect of the baseline resistance from the sensor on the output voltage by tuning a single reference element. Therefore, the error due to the mismatch in the resistors in the previous relaxation-oscillator-based circuits is eliminated.

2) Current Excitation: The conventional relaxation oscillator-based circuits, reported in [13]–[18], utilizes the square-wave output voltage signal for the excitation. Any variation/fluctuation in the amplitude of the square-wave voltage signal affects the accuracy of resistance measurement. In comparison, the proposed system utilizes a voltage-controlled current source in which the output current is independent of the fluctuation in the voltage - which results in an accurate system. Further, the current excitation-based topology provides uniform sensitivity in the resistance measurement over a wide range.

3) Design Analysis: In this paper, we provide a detailed analysis including the non-idealities of the circuit components for the resistance measurement. The detailed analysis and design criteria are missing in the previously reported relaxation oscillator-based interface circuits for resistance measurement. In addition to the design analysis, the analysis for the relative error, resolution, and sensitivity is also provided with the non-ideal operational amplifier. This helps in the selection of the circuit components as per the requirement of the sensor. Overall, the proposed circuit provides numerous advantages in comparison to the previous resistance-to-frequency converter circuit in terms of high accuracy, high sensitivity, and easy baseline resistance compensation.

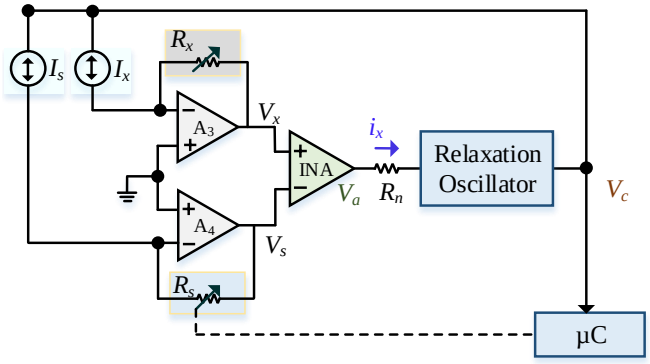

Fig. 2. The schematic diagram of the proposed signal conditioning circuit- the extended dynamic range interface.

II. The Proposed Circuit

The proposed circuit consists of a current generator & a half-bridge-based circuit followed by an instrumentation amplifier and relaxation oscillator circuit. Two configurations of the proposed circuit are designed. The first proposed circuit is based on a simple half-bridge circuit and the second proposed is based on a modified half-bridge topology for a wide dynamic range.

A. Basic Principle of Operation: The First Proposed Interface

The circuit diagram of the first proposed interface is shown in Fig. 1. Two bidirectional current generators I_x and I_s are used for exciting the sensor resistance R_x and reference resistance R_s. The bidirectional current generators are implemented using a reference current source (I_{src}) and diode bridge network, as shown in Fig. 1. The reference resistor is implemented using a digital potentiometer. The output V_a

of the instrumentation amplifier (INA) is proportional to the difference between R_x and R_s. The current i_x, proportional to V_a, flows through the relaxation oscillator and the oscillation frequency varies accordingly. The output square-wave signal of the relaxation-oscillator circuit acts as the clock pulse for the diode-based bidirectional current generator.

The operating principle of the proposed circuit is based on the change in the oscillation frequency of the relaxation oscillator due to incremental changes in the sensor resistance. The steps involved in the operating principle of the proposed circuit are as follows:

- First, the core relaxation oscillator circuit is designed to operate at a free running frequency of f_o by setting the current i_y. The i_x is zero during this phase.
- Afterwards, the half-bridge-based circuit is connected to the input of the relaxation oscillator, and current i_x is added with i_y. This changes the relaxation oscillator frequency from f_o to $f_o \pm f_b$, where f_b is proportional to the difference of R_x and R_s.
- Next, the reference resistor R_s is tuned equal to the baseline resistance by monitoring the oscillation frequency. When the oscillator frequency is equal to the free running frequency f_o, the baseline resistance of the sensor is compensated and current i_x becomes zero.
- Once the sensor is under the influence of the measurand, the incremental change in the sensor resistance ΔR due to the measurand changes the oscillation frequency from f_o to $f_o \pm \Delta f$.

1) Analysis for Oscillation Frequency: Considering $I_x(t) = I_s(t) = I(t)$ and unity-gain of the INA, the output voltage V_a of INA can be written as follows:

$$V_a = I(t)\ (R_x - R_s) \tag{1}$$

The clock signal for the current $I(t)$ is the output square wave of the relaxation oscillator circuit. However, the amplitude of the current is independent of the absolute value of the voltage V_c. The amplitude of the current $I(t)$ depends on the current source I_{src} and can be written as $G\,V_c$, where the value of G depends on I_{src}.

The current I_x; that is V_a/R_n: flows to the input of the relaxation oscillator. The voltage V_b at the output of the integrator can be derived as follows:

$$V_b(t) = -\frac{V_c}{C_i}\left[\frac{G\ (R_x - R_s)}{R_n} + \frac{1}{R_m}\right]\int_0^t dt \tag{2}$$

The threshold voltage of the Schmitt trigger is given as $V_c\,\frac{R1}{R_2}$. At $t = T/2$, the frequency; that is $f = 1/T$: of the square-wave output of the relaxation oscillator can be written as follows:

$$f = \frac{R_2}{4\,R_1\,R_m\,C_i} + \left(\frac{R_2}{4\,R_1\,R_m\,C_i}\right)(G(R_x - R_s)) \tag{3}$$

The expression for f can be simplified as follows:

$$f = f_o\ [1 + G\ (R_x - R_s)] \tag{4}$$

where f_o is the free-running oscillation frequency of the relaxation oscillator and can be written as follows:

$$f_o = \frac{R_2}{4\,R_1\,R_m\,C_i} \tag{5}$$

The change in the frequency of the relaxation oscillator can be written as follows:

$$\Delta F = \frac{R_2}{4\,R_1\,R_m\,C_i} G(\Delta R) \tag{6}$$

2) Dynamic Range: The current generator of the proposed circuit is implemented by the diode bridge and a current source I_{src} as shown in Fig. 1. The current I_x and I_s from the current generator flow through R_x and R_s, respectively. For a given current I_x & I_s values, the voltage V_x and V_s increase with the increase in the baseline resistance of the sensor. This limits the headroom voltage for the diodes to operate properly in the current generator. The conditions for the current generator to operate properly are:

$$|\mathrm{V_{AB}}| > (2.\mathrm{V_F} + \mathrm{V_{comp}}), \tag{7}$$

where V_F is the cut-in voltage of the diodes and V_{src} is the minimum operating voltage required across the current source IC for the operation. The high value of R_x and R_s limits the headroom for the voltage $|V_{AB}|$, and the condition of current generator Eq. (7) fails to meet. This affects the range of ΔR measurement. The maximum sensor resistor $R_{x,max}$ that can be used in Fig. 1 is given as follows:

$$R_{x,max} < \left(\frac{V_c - 2V_F - V_{src}}{I_x}\right) \tag{8}$$

3) Mismatch between Sensor and Reference Resistors: The mismatch in the two sensor resistances will result in an error in the measurement. Suppose δR is the mismatch between the resistances; the expression in the relaxation oscillator frequency can be analyzed as follows.

$$f = f_o[1 \pm G\delta R \pm G\Delta R] \tag{9}$$

where f_o is the relaxation oscillator frequency without half-bridge, ΔR is the change in the sensor resistance due to measurand, and G is the gain of the Instrumentation amplifier. The expression shows that the δR mismatch contributes to the frequency of the oscillator and results in the error. However, the effect of the mismatch can be calibrated at the start of the measurement by measuring the frequency without the influence of measurement. The shifted relaxation oscillator frequency can be assumed to be a new free-running frequency with the measurand zero.

B. Extended Dynamic Range: Second Proposed Interface

The circuit shown in Fig. 1 is improved to enhance the dynamic range. The improved interface circuit is shown in Fig. 2. The half-bridge configuration of the first-proposed solution is improved by introducing a trans-impedance amplifier using A_3 and A_4, as shown in Figure 2. Thanks to the negative feedback configuration of the trans-impedance amplifier, the voltage at node B of the current source is fixed at common-mode potential (ground for Fig. 2). Therefore, the voltage headroom for the current source is independent of the value of sensor resistance R_x. The maximum sensor resistor $R_{x,max}$

that can be used with the proposed current generator is given as follows:

$$R_x < \left(\frac{V_c}{I_{FCS}}\right) = R_{x,max} \tag{10}$$

The expression for the oscillation frequency for the extended interface shown in Fig. 2 is similar to the Fig. 1 and derived in Eq. (4).

Consider a case where $i_x = i_s = 100\mu A$ and $V_{DD} = \pm 5V$, the dynamic range of the circuit shown in Fig. 2 is at least twice than the circuit in Fig. 1.

C. Measurement Variation

The measured variation in this work is limited by two factors – 1) the supply voltage, 2) the DC non-idealities of the active components in the circuit, and 3) the parasitic capacitance and temperature drift.

1) Measurement range limitation due to supply voltage: – The output of the instrumentation amplifier is proportional to the change in the sensor resistance, magnitude of current sources, and the gain of the amplifier. The maximum output voltage of INA is limited by the supply voltage, which limits the measured variation range. Suppose the maximum output of the INA is $V_{(amax)}$; the maximum measured variation in the sensor resistance $R_{x(max)}$ for a single-element sensor can be derived as follows.

$$R_{x(max)} = V_{(a,max)}/(IG) + R_s \tag{11}$$

The voltage V_a generates a current i_x, which in turn changes the frequency of the relaxation oscillator. Therefore, the maximum variation in the oscillator's frequency is limited by the variation in the voltage of INA. The measured variation can be tuned by controlling the current and gain of the INA.

2) Measurement range limitation due to circuit non-idealities: The offset voltage and bias current of the INA also affect the measured variation and result in the error. Suppose the offset voltage is V_{of} and bias current is i_{bias}, the maximum variation in the sensor resistance for maximum output of the INA as $V_{(amax)}$, can be given as follows.

$$R_{x(max)} = \frac{V_{a,max} - GV_{of} - GI_{bias}(R_x - R_s)}{IG} + R_s \tag{12}$$

Therefore, the measured variation is limited by the nonidealities of active components. The DC non-idealities can be removed by using a DC-servo loop at the output of INA with a cut-off frequency lower than the minimum frequency of the relaxation oscillator.

3) Range variation limitation due to parasitic capacitance and temperature drift: A constant current $I = I_s = I_x$ flows through the sensor and generates a proportional voltage V_x. For an ideal sensor, the measurement range is limited by the maximum output of the INA for a given supply voltage. However, the presence of parasitic capacitance in parallel to the sensor resistance affects the measurement and limits the measured variation. The presence of parasitic capacitance and sensor resistance results in an exponential voltage V_a. The error due to parasitic capacitance is high when the oscillation period $(1/f)$ is comparable to the RC time constant of the parasitic capacitance and sensor resistance. Therefore the oscillation frequency needs to be chosen according to the value of measurement variation and parasitic capacitance value.

Another important factor which affects the measured variation and well as the error in the measurement is the temperature drift. The variation in the temperature may result in a thermoelectric offset in the circuit which can be filtered out by using a DC-servo loop. In addition, the drift in the sensor resistance due to temperature can be compensated using neural networks [22].

III. Nonideal Performance Analysis

The frequency of the relaxation oscillator circuit is affected by the nonideal behavior of the circuit components. To understand the design flow for the specific sensing requirement and observe the effect of the circuit components, we introduce the nonidealities of an operational amplifier and a comparator into the performance analysis of the relaxation oscillator. Nonidealities of an operational amplifier are the finite gain-bandwidth product (GBP), the offset voltage, and the slew rate.

The steps for the nonideal performance analysis are as follows:

1) First, we will analyze the effect of the gain-bandwidth product (GBP) on the slope of the integrators' output voltage.
2) Next, in addition to the GBP, the effect of the input-offset voltage and bias-current of the operational amplifiers on the slope of the integrator will be analyzed.
3) The high and low periods of the square-wave output of the relaxation oscillator will be derived from the slope of the integrator and the threshold voltage of the Schmitt trigger. The non-idealities of the Schmitt trigger such as the rise and fall time will be added in the high and low periods of the square-wave signal.
4) The frequency of the square-wave output of the relaxation oscillator will be obtained from the derived expression of the time period.
5) The error in the resistance measurement due to component non-idealities will be obtained from the derived expression of frequency. The selection of components for designing the proposed circuit will be introduced.

Each step for the design analysis of the proposed circuit is analyzed in detail as follows:

1) Effect of GBP on Slope of Integrator: The finite GBP of the operational amplifier can be written as follows:

$$A(s) = \frac{A_0\,\omega_0}{s + \omega_0} \approx \frac{A_0\,\omega_0}{s} \tag{13}$$

where A_0 is the DC gain, ω_0 is the dominant-pole, and $A_0\omega_0$ is the gain-bandwidth product. Using this, the output voltage of the integrator when driven by a unit step voltage $\mathrm{V_p}$ can be derived as follows:

$$V_a(s) = \frac{-A_0\,\omega_0}{s^2}\frac{V_p(G\Delta R + 1)}{R_i C_i}\left(\frac{1}{s + \dfrac{2 + A_o\omega_0 R_i C_i}{R_i C_i}}\right) \tag{14}$$

$$V_R(t) = \frac{R_1}{R_2}V_p - \frac{V_p + I_s\Delta R}{R_i C_i}\Bigg\{ \overbrace{\frac{t}{\left(1+\frac{2}{A_0\omega_0 R_i C_i}\right)}}^{\text{Integration slope reduction due to finite GBW}} \underbrace{- \frac{1}{\left(1+\frac{2}{A_0\omega_0 R_i C_i}\right)^2}\frac{1}{A_0\omega_0}\left[1-e^{-\left(\frac{2+A_o\omega_0 R_i C_i}{R_i C_i}\right)t}\right]}_{\text{Offset voltage due to finite GBW}} \Bigg\} \quad (15)$$

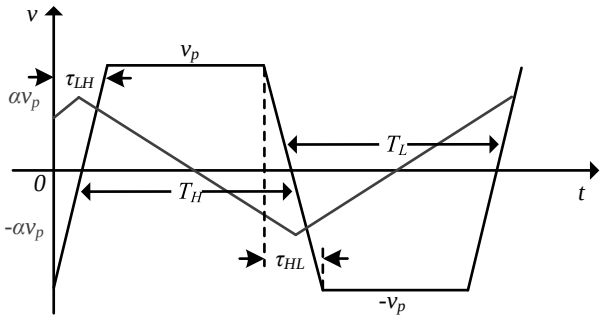

Fig. 3. Waveform of the relaxation oscillator considering the response delay of comparator

The equivalent time-domain expression of $V_a(s)$ is derived in Eq. (15). The first term denotes the initial starting point of the slope of $V_a(t)$. The first term inside the braces indicates that the finite GBP of the operational amplifier A_1 reduces the slope of $V_a(t)$. The second term inside the braces represents the offset voltage due to finite GBP. The effect of each term is analytically evaluated for different operational amplifier integrated circuits. The effect of the transient term is found to be negligible and can be neglected. The expression of the slope of $V_a(t)$ can be written from Eq. (15) as follows:

$$SL = min\left\{\frac{V_p}{R_i C_i}\left(1+\frac{\Delta R}{R_p}\right)\frac{1}{\left(1+\frac{2}{A_0\omega_0 R_i C_i}\right)}, SR\right\} \quad (16)$$

where $R_p = 1/G$.

2) Combined effect on Slope of Integrator Due to GBP and Offset-Voltages: A similar analysis shows that the input offset voltage of the operational amplifiers simply shifts the voltage V_p by the effective offset voltage. Considering $V_{o,ina}$ is the input-offset voltage of the INA. $V_{o,A1}$, $V_{o,A2}$,$V_{o,A3}$, and $V_{o,A2}$ are the input-offset voltage of operational-amplifiers A_1, A_2, A_3, and A_4, respectively. i_b is the input-bias current of A_1. The modified expression of the slope, considering the GBP, input-offset voltage, and bias-current of the operational amplifier and INA, can be written as follows:

$$SL = min\left\{\frac{V_p}{R_i C_i}\left(1+\frac{\Delta R}{R_p}\pm\frac{V_{off}}{V_p}\right)\frac{1}{\left(1+\frac{2}{A_0\omega_0 R_i C_i}\right)}, SR\right\} \quad (17)$$

where $V_{off} = V_{o,ina}+V_{o,A1}+V_{o,A2}+V_{o,A3}+V_{o,A2}+i_b R_i/2$.

3) The High and Low Period of Square-Wave: The expression of the high and low time period, T_H & T_L, respectively, are derived from the expression of slope in Eq. (17). Referring to the waveform in Fig. 3, the expressions of T_H and T_L can be obtained using the slope of the positive and negative going ramp, $SL_{(+)}$ $SL_{(-)}$, respectively. Considering, τ_{LH} as the low-to-high and τ_{HL} as the high-to-low response delay of the Schmitt-trigger (A_2), the expressions for T_L and T_H can be derived from Fig. 3 as follows:

$$T_L = \frac{(2\alpha+\gamma)V_p}{SL_{(+)}} + \frac{\tau_{LH}+\tau_{HL}}{2} \quad (18)$$

$$T_H = \frac{(2\alpha+\gamma)V_p}{SL_{(-)}} + \frac{\tau_{HL}+\tau_{LH}}{2} \quad (19)$$

where $\alpha = R_1/R_2$ and γ denotes the offset component due to finite GBP in Eq. (15)

$$\gamma = \frac{1}{\left(1+\frac{2}{A_0\omega_0 R_i C_i}\right)^2}\frac{1}{A_0\omega_0}. \quad (20)$$

Assuming the response time of the Schmitt trigger is equal, the expression for the Time (T) of the square-wave signal of the relaxation oscillator circuit can be written as follows:

$$T = 2\left(2\alpha+\gamma\right)\left(R_i C_i\right)\left(1+\frac{2}{A_0\omega_0 R_i C_i}\right)\left(\frac{1}{1+\frac{\Delta R}{R_p}}\right) \times\left[\frac{1}{1-k_{o,e}^2}\right]+2\tau \quad (21)$$

where $k_{o,e} = \left(\frac{V_{of}}{V_p}\right)\left(1+\frac{\Delta R}{R_p}\right)$

The effect of the response delay can be neglected since high-speed comparator integrated circuits are available. Consider a comparator with a response delay of 10 ns. The maximum error in the measurement due to the response delay for a relaxation oscillator running at a frequency of 5 kHz is small. It can be neglected by utilizing the high-speed comparator.

4) Frequency of Square-Wave Output: From Eq. 21, the frequency of the square-wave output of the converter can be written as follows:

$$F = \left(1+\frac{\Delta R}{R_p}\right)\left[\frac{1}{2\left(2\alpha+\gamma\right)\left(R_i C_i\right)\left(1+\frac{2}{A_0\omega_0 R_i C_i}\right)}\right]\left(1-k_{o,e}^2\right) \quad (22)$$

The change in the frequency ΔF due to ΔR can be derived from Eq. 22 as follows:

$$\Delta F = \left(\frac{\Delta R}{R_p}\right)\left[\frac{1}{2\left(2\alpha+\gamma\right)\left(R_i C_i\right)\left(1+\frac{2}{A_0\omega_0 R_i C_i}\right)}\right]\left(1-k_{o,e}^2\right) \quad (23)$$

The expression indicates that the value of ΔF depends on the circuit parameters. Therefore, the selection of the circuit

TABLE I
OPERATIONAL AMPLIFIERS WITH PERFORMANCE PARAMETERS

Op-Amp IC	GBP (MHz)	SR ($V/\mu s$)	Vof (mV)	i_b (nA)	τ (ns)
LM741	1.5	0.7	5	500	300
TL071	5.25	29	4	0.1	310
LTC1151	2	2.5	0.005	0.1	–
LT1049	0.8	0.8	0.01	0.05	–
OPA177	0.6	0.3	0.6	6	–

components needs to be carefully done for the proposed circuit as per the sensing requirement.

IV. DESIGN CRITERIA

In this section, we will discuss the design criteria such as the relative error, resolution, and sensitivity considering the non-idealities of the circuit components.

A. Relative Error

The error in ΔR measurement due to the non-idealities of the circuit components can be derived as follows:

$$\epsilon = \frac{\Delta R_{true} - \Delta R_{measured}}{\Delta R_{true}} \tag{24}$$

where ΔR_{true} is the ideal value of resistance from expression (ideal) and $\Delta R_{measured}$ is the value of ΔR with the component non-idealities from expression (22). The error in the ΔR can be derived as follows:

$$\epsilon = \Big[1 - \frac{1}{\Big(1 - \frac{\gamma}{2\alpha}\Big)\Big(1 + \frac{2}{A_0\omega_0 R_i C_i}\Big)}\Big]\Big[1 - \Big(\frac{V_{of}}{V_p}\Big)^2\Big(1 + \frac{\Delta R}{R_p}\Big)^2\Big] \tag{25}$$

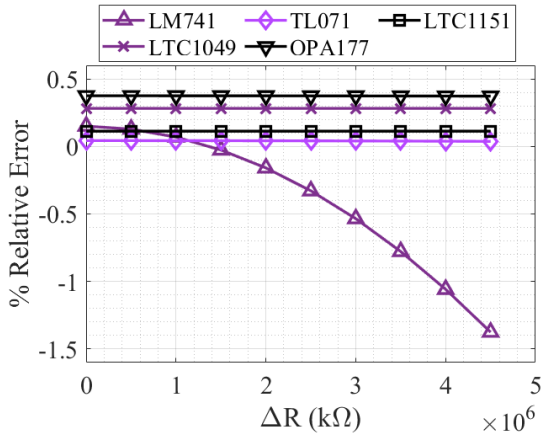

Fig. 4. Percentage relative error for different values of ΔR

B. Sensitivity

The sensitivity of the proposed system shown in Fig. 2 is analytically derived from Eq. 22 as follows:

$$\frac{\delta F}{\delta \Delta R} = \Big[\frac{1}{2R_p\,(2\alpha+\gamma)\,(R_i C_i)\,\Big(1 + \frac{2}{A_0\omega_0 R_i C_i}\Big)}\Big]\Big(1 - k_{o,s}\Big) \tag{26}$$

TABLE II
COMPONENTS FOR THE PROTOTYPE PCB

Component	Module	Function
A_1, A_2, A_3, A_4	LTC1151	Operational Amplifier
I_{src}	LM334	Current Source
D_1, D_2, D_3, D_4	UC3611	Schottky Diode Bridge
R_s	AD5242BRUZ10	Digital-Potentiometer
INA	INA333	Instrumentation Amplifier
μC	ESP32/MSP430	Micro-controller
R_m, R_n	1 MΩ	Resistors
R_1	4.7 kΩ	Resistor
R_2	10 kΩ	Resistor
C_i	1 nF	Capacitor

where $k_{o,s} = \Big(\frac{V_{of}}{V_p}\Big)^2\Big[\Big(1 + \frac{\Delta R}{R_p}\Big)^2 + 2\Big(1 + \frac{\Delta R}{R_p} + \frac{\Delta R^2}{R_p^2}\Big)\Big]$

The derived solution for the sensitivity is plotted for different ΔR values in Fig. 5. The figure shows that the sensitivity is almost constant for the wide variation in the ΔR values. The operational amplifier LM741 has an input-offset voltage of 5 mV. The higher value of input-offset voltage affects the sensitivity of the circuit at higher ΔR values as derived in Eq. 26. Therefore, a low-offset voltage operational amplifier is preferred for better sensitivity over a wide-range ΔR measurement.

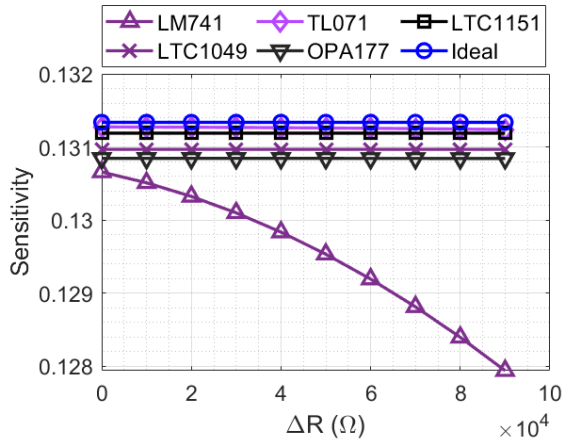

Fig. 5. Percentage relative error for different values of ΔR

V. EXPERIMENT SETUP AND RESULTS

A prototype of the proposed circuit shown in Fig. 2 is fabricated and tested. The components used for the fabrication of the prototype PCB are listed in Table IV-B. The circuit is powered with a single supply of $5\,V$. A photograph of the fabricated PCB is shown in Fig. 6. The waveform at different nodes of the circuit is shown in Fig. 7. The procedure for the experiment is as follows:

1) First, the relaxation oscillator is set to the free-running frequency f_o before connecting the half-bridge. The frequency f_o is set by appropriately choosing the values of the integrator and Schmitt trigger's components. The frequency f_o is set equal to 200 Hz.
2) Connect the half-bridge circuit to the relaxation oscillator. The frequency of the oscillator is shifted due to the baseline resistance of the sensor.

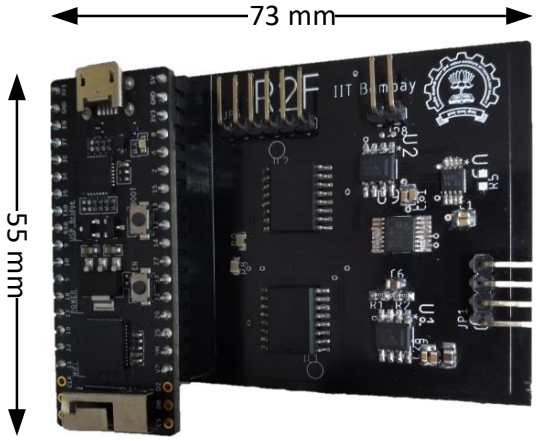

Fig. 6. Photograph of the fabricated PCB

3) The digital potentiometer such that it compensates for the baseline resistance of the sensor by monitoring the frequency of the relaxation oscillator.
4) Once the relaxation oscillator frequency is set back to f_o, the sensor is placed under the influence of the measurand, and the incremental change in the frequency is recorded.

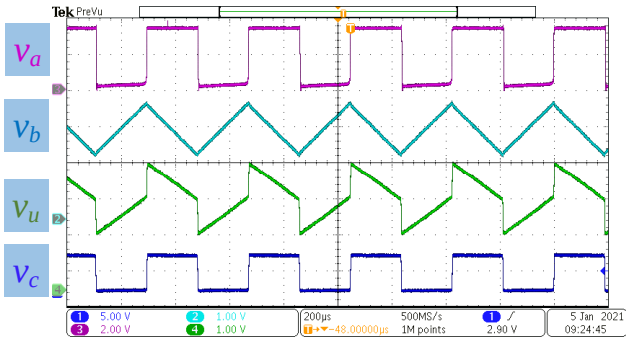

Fig. 7. Waveform at different node of the circuit shown in Fig. 2

A. Measurement with Emulated Sensor

Multiple experiments were conducted to demonstrate the effectiveness of the proposed technique using the emulated sensor. The sensor is emulated using discrete components. The performance of the proposed signal conditioning is tested for the dynamic range for the circuits shown in Fig. 1 and Fig. 2. In addition, the performance of the proposed circuit is tested for different values of the sensor's baseline resistance.

1) Dynamic-Range Test: In this experiment, the dynamic range of both the proposed interface circuits is tested. The currents i_s and i_x are set equal to 100 μA both. The limit for the maximum measurement range for the proposed signal conditioning circuits shown in Fig. 1 and Fig. 2 are given by Eq. 8 and Eq. 10, respectively. The measurement range can be further enhanced using by reducing the value of the current sources. The programmable current source LM334 can be used to enhance the range of measurement. A digital potentiometer is used with LM334 to program the current source using a microcontroller.

The result shows that the proposed circuit can measure a sensor resistance up to 22 kΩ and 48 kΩ using the circuit shown in Fig. 1 for currents i_s and i_x equals to 100 μA. Moreover, for currents i_s and i_x equals to 10 μA, the measurement range is extendable up to 500 kΩ for the circuit shown in Fig. 2.

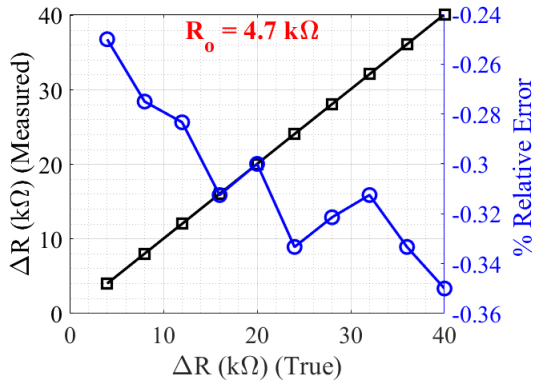

Fig. 8. Percentage relative error for different values of ΔR

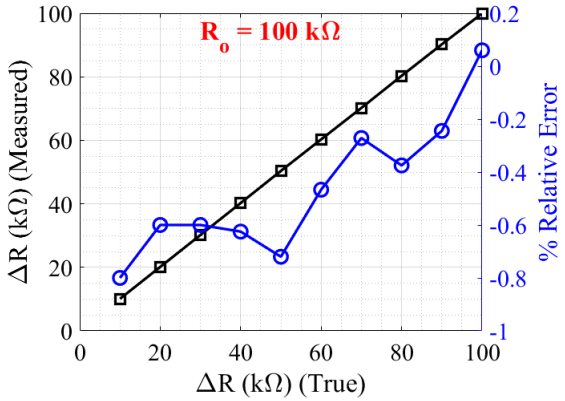

Fig. 9. Percentage relative error for different values of ΔR

2) Experiment with different-baseline resistance: The proposed circuit shown in Fig. 2 is tested for different values of the baseline resistor of the sensor. The baseline resistance of the sensor is emulated by placing a discrete resistor. The effect of the baseline resistance of the sensor is compensated at the beginning of the measurement cycle by using the digital potentiometer (R_s).

The experimental results for the baseline resistance of 4.7 kΩ and 100 kΩ are shown in Fig. 8 and Fig. 9, respectively. The value of ΔR is varied from 4 kΩ to 40 kΩ for a baseline resistance of 4.7 kΩ and 10 kΩ to 100 kΩ for a baseline resistance of 100 kΩ. The maximum percentage relative error is less than $\pm$ 1%.

This article has been accepted for publication in IEEE Sensors Journal. This is the author's version which has not been fully edited and content may change prior to final publication. Citation information: DOI 10.1109/JSEN.2024.3429246

B. Measurement with Resistive Humidity Sensor

The performance of the proposed circuit is also tested with a commercial resistive humidity sensor HS12SP from Talaire. The sensor is placed inside a humidity test chamber along with a reference humidity sensor DHT22. The measurement result of the test is plotted in Fig. 10. The results show that the proposed circuit is able to measure the sensor parameters accurately in comparison with the reference sensors.

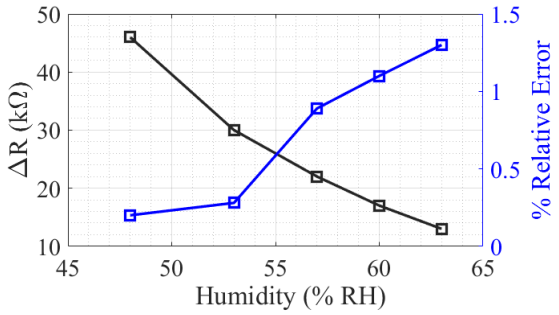

Fig. 10. ΔR measurement and percentage relative error for different humidity levels

C. Performance Analysis

The performance parameters such as the standard deviation and signal-to-noise ratio (SNR) of the proposed circuit are obtained experimentally. A total of 500 samples were recorded for a ΔR equal to 47 kΩ, and the value of the performance parameters is obtained from the recorded data points as per [23]. The result shows that the proposed circuit can provide SNR of 80 dB with a standard deviation of around 30 Ω for ΔR value of 47 kΩ.

The measurement range of the relaxation-oscillator-based circuit with a bridge-based front end is proportional to the supply voltage. A wider measurement range can be obtained with a large supply voltage. However, it will increase the power consumption of the system. Moreover, the large supply voltage affects the portability of the system. The developed circuit has a 5 V supply and can be powered with a miniaturized battery.

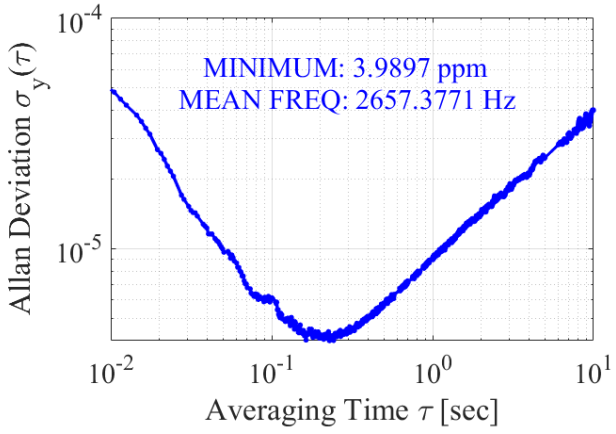

Fig. 11. Allan deviation plot of the designed relaxation oscillator.

TABLE III
PERFORMANCE PARAMETERS OF THE DEVELOPED SYSTEM

Parameters	Expression	Value
SD(σ)	$\sqrt{\sum_{n=1}^{M} \frac{(S(n)-\overline{S})^2}{M-1}}$	30.4 Ω
SNR	$10 \log \frac{\sum_{n=1}^{M}(S(n))^2}{\sum_{n=1}^{M}(S(n)-\overline{S})^2}$	80.26 dB

Allan deviation of the developed circuit is obtained using a frequency counter (53220A from Keysight) for a ΔR value of around 25 kΩ. The plot of the obtained Allan deviation is shown in Fig. 11. The result shows that the circuit is able to measure the ΔR value with a resolution of around 4 ppm.

VI. Performance Comparison and Discussion

The performance of the proposed circuit is compared with other resistance measurement circuits reported in the literature. In comparison to the reported work, the following features of the proposed circuit can be highlighted:

1) The proposed circuit is based on a relaxation oscillator and provides output in the form of change in the frequency with respect to the measurand. This output is a quasi-digital signal which provides high noise immunity.
2) The proposed circuit is based on a half-bridge topology with current excitation. The half-bridge topology allows for easily compensating the baseline resistance by tuning a single reference resistor. A digital potentiometer is utilized to implement the reference resistor which provides automatic compensation of the baseline resistance at the beginning of the measurement.
3) As compared to the other reported work in Table IV where in all the cases a dual-supply of minimum ±5 V is utilized, the proposed circuit utilizes a supply voltage of 5 V. Thanks to this, the overall power consumption of the proposed circuit is lowest in the Table IV.
4) The measurement range and sensitivity of the proposed circuit are tunable and can be adjusted easily by varying the amplitude of the current source and gain of the instrumentation amplifier.
5) Thanks to the relaxation oscillator-based interface, the minimum bandwidth of the proposed circuit is 200 Hz. Therefore, the measurement time of the proposed circuit is significantly lower than the other reported works in Table IV.

The proposed circuit can be used for the single-element resistive sensors as well as half-bridge topology. For single element sensor, the other branch can be integrated with a auto-zeroing loop and a voltage-controlled resistance. The bridge can be either deflection-based or balanced by an auto-balancing approach such as the one earlier reported in [9], [10], [24] - which could result in higher accuracy.

The oscillator frequency is measured from 200 Hz to 2 kHz for the given sensor resistance. We understand measuring the phase noise is very critical to further understand the limitations of the oscillator circuits. The future work would be to measure the phase noise of the circuit and integration of proposed

TABLE IV
PERFORMANCE COMPARISON OF THE PROPOSED CIRCUIT

	[25]	[9]	[14]	[26]	[6]	[27]	This work
Excitation signal	Voltage	Voltage	Voltage	Voltage	Current	Current	Current
Output type	Digital	Voltage	Frequency	Voltage	Voltage	Voltage	Frequency
Excitation range	Fixed 1 V	Fixed 1V	Fixed	–	Fixed 50 μA	Fixed 1 μA	Programmable 1 μA
Measurement	ΔR	R (Absolute)	ΔR	$\Delta R/R$	R (Absolute)	ΔR	ΔR
Supply	$\pm$ 5V	$\pm$ 7V	$>\pm$ 5V	$\pm$ 12V	$\pm$ 12V	$\pm$ 5V	5 V
Resistance Range	–	–	55 Ω	–	8 kΩ - 230 kΩ	100 Ω - 4 MΩ	$<$50 kΩ @ 100μA $<$500 kΩ @ 10 μA
Sensor Excitation	On-board	External	On-board	External	On-board	On-board	On-board
Baseline compensation	Automatic	On-board	Manual	Automatic	NA	NA	Automatic
Programmable range & Sensitivity	No	No	Yes	No	No	No	Yes
Power Consumption*	–	–	–	720 mW	–	420 mW	40 mW
Bandwidth	0.35 Hz#	2 Hz	–	0.45 Hz	NA	4 Hz	200 Hz

: Power consumption of the interface circuit, #: Bandwidth is calculated from the measurement time

technique with the three and four lead wire methods for remote sensors.

VII. CONCLUSION

A half-bridge and relaxation oscillator based ΔR to frequency converter circuit for resistive sensors is presented in this paper. The half-bridge configuration of the proposed circuit provides differential operation between the sensor resistor and a programmable reference resistor to compensate for the baseline resistance of the sensor. The half-bridge configuration and relaxation oscillator allow high-resolution measurement of the sensor resistance. A prototype of the circuit is developed and tested. The result shows that the developed board is able to measure the sensor resistance over a wide range with high resolution. The proposed circuit is an excellent replacement for the Wheatstone-bridge-based signal conditioning circuit for single-element resistive sensors. The performance parameters of the developed circuit show that the performance of the proposed circuit in terms of resolution, power consumption, and bandwidth is better than the other reported circuits for resistive sensors.

REFERENCES

[1] L. Baxter, *Capacitive Sensors Design and Application*. New Delhi, India: Wiley-IEEE Press, 1997.

[2] A. D. Marcellis and G. Ferri, *Analog Circuit and System for Voltage-mode and Current-mode Sensor Interfacing Application,*. New Delhi, India: Springer, 2011.

[3] S. Oh, Y. Lee, J. Wang, Z. Foo, Y. Kim, W. Jung, Z. Li, D. Blaauw, and D. Sylvester, "A dual-slope capacitance-to-digital converter integrated in an implantable pressure-sensing system," *IEEE Journal of solid-state circuits*, vol. 50, no. 7, pp. 1581–1591, July 2015.

[4] Z. H. Zargar and T. Islam, "A novel cross-capacitive sensor for noncontact microdroplet detection," *IEEE Trans. Indus. elec.*, vol. 66, no. 6, pp. 4759–4766, June 2019.

[5] J. Fraden, *Handbook of Modern Sensors: Physics, Designs, and Applications*. New Delhi, India: Springer, 2010.

[6] K. Kishore, S. Malik, M. S. Baghini, and S. A. Akbar, "A dual-differential subtractor-based auto-nulling signal conditioning circuit for wide-range resistive sensors," *IEEE Sensors Journal*, vol. 20, no. 6, pp. 3047–3056, 2020.

[7] R. Pallas-Areny and W. John G., *Sensors and Signal Conditioning*. wiley, 2020, vol. 2.

[8] A. De Marcellis, G. Ferri, and P. Mantenuto, "Analog wheatstone bridge-based automatic interface for grounded and floating wide-range resistive sensors," *Sensors and Actuators B: Chemical*, vol. 187, pp. 371 – 378, 2013, selected Papers from the 14th International Meeting on Chemical Sensors. [Online]. Available: http://www.sciencedirect.com/science/article/pii/S0925400512013536

[9] S. Malik, M. Ahmad, L. Somappa, T. Islam, and M. S. Baghini, "AN-Z2V: autonulling-based multimode signal conditioning circuit for r-c sensors," *IEEE Transactions on Instrumentation and Measurement*, vol. 69, no. 11, pp. 8763–8772, 2020.

[10] P. Mantenuto, A. D. Marcellis, and G. Ferri, "Novel modified de-sauty autobalancing bridge-based analog interfaces for wide-range capacitive sensor applications," *IEEE Sensors J.*, vol. 14, no. 5, pp. 1664–1672, May 2014.

[11] S. Malik, L. Somappa, M. Ahmad, and M. S. Baghini, "An-c2v: An auto-nulling bridge-based signal conditioning circuit for leaky capacitive sensors," *IEEE Sensors Journal*, vol. 20, no. 12, pp. 6432–6440, 2020.

[12] M. Verhelst and A. Bahai, "Where analog meets digital: Analog?to?information conversion and beyond," *IEEE Solid-State Circuits Magazine*, vol. 7, no. 3, pp. 67–80, 2015.

[13] A. Cichocki and R. Unbehauen, "A switched-capacitor interface for capacitive sensors based on relaxation oscillators," *IEEE Trans. Instrum. Meas.*, vol. 39, no. 5, pp. 797–799, Oct. 1990.

[14] A. D. Marcellis, A. Depari, G. Ferri, A. Flammini, D. Marioli, V. Stornelli, and A. Taroni, "A CMOS integrable oscillator-based front end for high-dynamic-range resistive sensors," *IEEE Trans. Instrum. Meas.*, vol. 57, no. 8, pp. 1596–1604, Aug. 2008.

[15] H. Ganesan, B. George, and S. Aniruddhan, "A relaxation oscillator based interface circuit for lvdt," in *2018 IEEE International Instrumentation and Measurement Technology Conference (I2MTC)*, 2018, pp. 1–5.

[16] K. Mochizuki, K. Watanabe, T. Masuda, and M. Katsura, "A relaxation-oscillator-based interface for high-accuracy ratiometric signal processing of differential-capacitance transducers," *IEEE Trans. Instrum. Meas.*, vol. 47, no. 1, pp. 11–14, Feb. 1998.

[17] H. Shibata, M. Ito, M. Asakursa, and K. Watanabe, "A digital hygrometer using a polyimide film relative humidity sensor," *IEEE Transactions on Instrumentation and Measurement*, vol. 45, no. 2, pp. 564–569, 1996.

[18] T. Islam, A. U. Khan, and J. Akhtar, "Accuracy analysis of oscillator-based active bridge circuit for linearly converting resistance to frequency," in *IMPACT-2013*, 2013, pp. 305–309.

[19] T. Islam and M. Zia-Ur-Rahman, "Investigation of the electrical characteristics on measurement frequency of a thin-film ceramic humidity sensor," *IEEE Trans. Instrum. Meas.*, vol. 65, no. 3, pp. 694–702, March 2016.

[20] V. Ferrari, A. Ghisla, Z. K. Vajna, D. Marioli, and A. Taroni, "Asic front-end interface with frequency and duty cycle output for resistive-bridge sensors," *Sensors and Actuators A: Physical*, vol. 138, no. 1, pp. 112 – 119, 2007. [Online]. Available: http://www.sciencedirect.com/science/article/pii/S0924424707003354

[21] S. Dalola, V. Ferrari, and D. Marioli, "Micromachined piezoresistive inclinometer with oscillator-based integrated interface circuit and tem-

perature readout," *Measurement Science and Technology*, vol. 23, no. 3, p. 035107, feb 2012.

[22] B. Yao, Y. Dai, G. Xia, Z. Zhang, and J. Zhang, "High-sensitivity and wide-range resistance measurement based on self-balancing wheatstone bridge and gated recurrent neural network," *IEEE Transactions on Industrial Electronics*, vol. 70, no. 5, pp. 5326–5335, 2023.

[23] L. Xu, S. Sun, A. Cao, and W. Yang, "Performance analysis of a digital capacitance measuring circuit,," *Rev. Sci. Instrum.*, vol. 86, no. 5, p. p. 054703, 2015.

[24] A. D. Marcellis, G. Ferri, and P. Mantenuto, "A novel 6-decades fully-analog uncalibrated wheatstone bridge-based resistive sensor interface," *Sens. Actuators B, Chm.*, vol. 189, no. 1, pp. 130–140, Feb. 2013.

[25] V. Sreenath, K. Semeerali, and B. George, "A resistive sensor readout circuit with intrinsic insensitivity to circuit parameters and its evaluation," *IEEE Transactions on Instrumentation and Measurement*, vol. 66, no. 7, pp. 1719–1727, 2017.

[26] S. Nag, N. S. Kale, V. R. Rao, and D. K. Sharma, "An ultra-sensitive r/r measurement system for biochemical sensors using piezoresistive micro-cantilevers," in *2009 Annual International Conference of the IEEE Engineering in Medicine and Biology Society*, 2009, pp. 3794–3797.

[27] V. S. Palaparthy, S. N. Doddapujar, G. Gupta, P. Das, S. A. Chandorkar, S. Mukherji, M. S. Baghini, and V. R. Rao, "E-nose: Multichannel analog signal conditioning circuit with pattern recognition for explosive sensing," *IEEE Sensors Journal*, vol. 20, no. 3, pp. 1373–1382, 2020.